Geophysical Journal International

Geophys. J. Int. (2010) **180,** 685–696 doi: 10.1111/j.1365-246X.2009.04445.x

Upper crustal structure of an active volcano from refraction/reflection tomography, Montserrat, Lesser Antilles

M. Paulatto,[1] T. A. Minshull,[1] B. Baptie,[2] S. Dean,[1] J. O. S. Hammond,[3] T. Henstock,[1] C. L. Kenedi,[4] E. J. Kiddle,[3] P. Malin,[4] C. Peirce,[5] G. Ryan,[4,6] E. Shalev,[4] R. S. J. Sparks[3] and B. Voight[7]

[1]*National Oceanography Centre, Southampton* SO14 3ZH, *UK. E-mail: m.paulatto@noc.soton.ac.uk*
[2]*British Geological Survey, West Mains Road, Edinburgh* EH9 3LA, *UK*
[3]*Department of Earth Science, University of Bristol, Queen's Road, Bristol* BS8 1RJ, *UK*
[4]*Institute of Earth Science and Engineering, University of Auckland, Private Bag* 92019, *Auckland* 1142, *New Zealand*
[5]*Department of Earth Sciences, Durham University, South Road, Durham* DH1 3LE, *UK*
[6]*Montserrat Volcano Observatory, Flemmings, Montserrat, MSR*
[7]*Department of Geosciences, Penn State University,* 503 *Deike Building, University Park, PA* 16802, *USA*

Accepted 2009 November 3. Received 2009 September 1; in original form 2009 May 6

SUMMARY

To better understand the volcanic phenomena acting on Montserrat, the SEA-CALIPSO seismic experiment (Seismic Experiment with Airgun-source – Caribbean Andesitic Lava Island Precision Seismo-geodetic Observatory) was conducted in 2007 December with the aim of imaging the upper crust and the magmatic system feeding the active Soufriére Hills Volcano. The 3-D survey covered an area of about 50 × 40 km and involved the deployment of 247 land stations and ocean-bottom seismometers (OBSs). A subset of the data, recorded by four OBSs and four land stations on a southeast to northwest line, has been analysed, and traveltimes have been inverted to obtain a 2-D seismic velocity model through the island. Inverted phases include crustal and sediment *P* waves and wide-angle reflections. The resulting velocity model reveals the presence of a high velocity body (3.5–5.5 km s^{-1}) beneath the island, with highest velocities beneath the Soufriére and Centre Hills, corresponding primarily to the cores of these volcanic edifices, built of a pile of andesite lava domes and subsequent intrusions. In the offshore region, velocities in the surficial sediment layer vary from 1.5 to 3.0 km s^{-1}, consistent with a mainly calcareous and volcaniclastic composition. A wide-angle reflector is observed at a depth of ∼1200 m below the seabed, and appears to deepen beneath the island. The upper crust beneath this reflector has velocities of 4.0–6.0 km s^{-1} and is inferred to correspond to plutonic and hypabyssal rocks and sedimentary material of the old arc. The high velocity region beneath the island, extends into the crust to a depth of at least 5 km, and is believed to be caused by an intrusive complex, possibly of intermediate composition. A low velocity zone, as would be expected in the presence of an active magma chamber, was not observed perhaps due to the limited resolution beneath ∼5 km depth. Our results so far provide the first wide-angle seismic constraints on the upper crustal structure of the island to a depth of 10 km, and will help understanding the processes that drive volcanism at Montserrat and other island arc volcanoes.

Key words: Controlled source seismology; Seismic tomography; Volcano seismology; Volcanic arc processes; Crustal structure; Volcano monitoring.

1 INTRODUCTION

The seismic velocity structure of island arc volcanoes derived from seismic experiments, complemented by direct measurements of seismic velocities of crustal rocks, can provide constraints on the petrology and chemical composition of arc crust. Further it provides insights on the mechanisms by which, and the extent to which, regions of intermediate composition are developed within primarily basaltic crust at inter-oceanic arcs. Large-scale seismic experiments have been conducted in recent years in the Izu-Bonin arc (Kodaira *et al.* 2007), the Mariana arc (Takahashi *et al.* 2007; Calvert *et al.* 2008), the Aleutian arc (Shillington *et al.* 2004; Van Avendonk *et al.*

2004) and the southern Lesser Antilles arc (Christeson *et al.* 2008). These studies have shown that intra-oceanic arc crust has characteristics that are intermediate between continental and oceanic crust, and that there is great along-arc variability in crustal thickness and average seismic velocity. In 2007 December the SEA-CALIPSO experiment, a smaller scale 3-D active-source seismic survey, was conducted to investigate the upper crustal structure of Montserrat (Fig. 2) and its magmatic system. Here we present the first seismic velocity model of the island derived from the inversion of a subset of the data collected, the first detailed image of an island arc volcano in the Lesser Antilles. Our results will complement other geophysical and geological observations, in an attempt to better understand the processes that drive the volcanic activity in Montserrat.

1.1 Geological setting

Montserrat (16°45′N, 62°12′W) lies in the northern half of the Lesser Antilles arc, between Guadeloupe and Nevis (Fig. 1). Here the island arc is divided into two parallel branches, an external (eastern) arc and an internal (western) arc. The external arc was active between the early Eocene (∼55 Ma) and the mid Oligocene (∼30 Ma) and is now extinct and mostly overlain by carbonate sediments. A 10 Myr period without volcanic activity followed the extinction of the older arc which lasted until about 22 Ma when volcanism resumed along the line of what is now the inner volcanic arc (Bouysse *et al.* 1990). The oldest volcanic rocks on Montserrat date back to 2.6 Ma (Harford *et al.* 2002) but the volcanic centre was probably active as a submarine volcano before this.

Montserrat is 16 km long and 10 km wide and consists almost entirely of volcanic deposits. The island is made up of three major volcanic centres: in the north lie the extinct and heavily eroded Silver Hills (*ca*. 2.6–1.2 Ma); in the centre lie the Centre Hills (*ca*. 950–550 ka), also extinct and crossed by deep erosive canyons; and in the south lies the massif comprising South Soufriére Hills (*ca*. 135–125 ka) and Soufriére Hills (*ca*. 170 ka to present) (Harford *et al.* 2002). The upper structure of the Soufriére Hills Volcano is composed of a set of andesitic domes surrounded by a cloak of

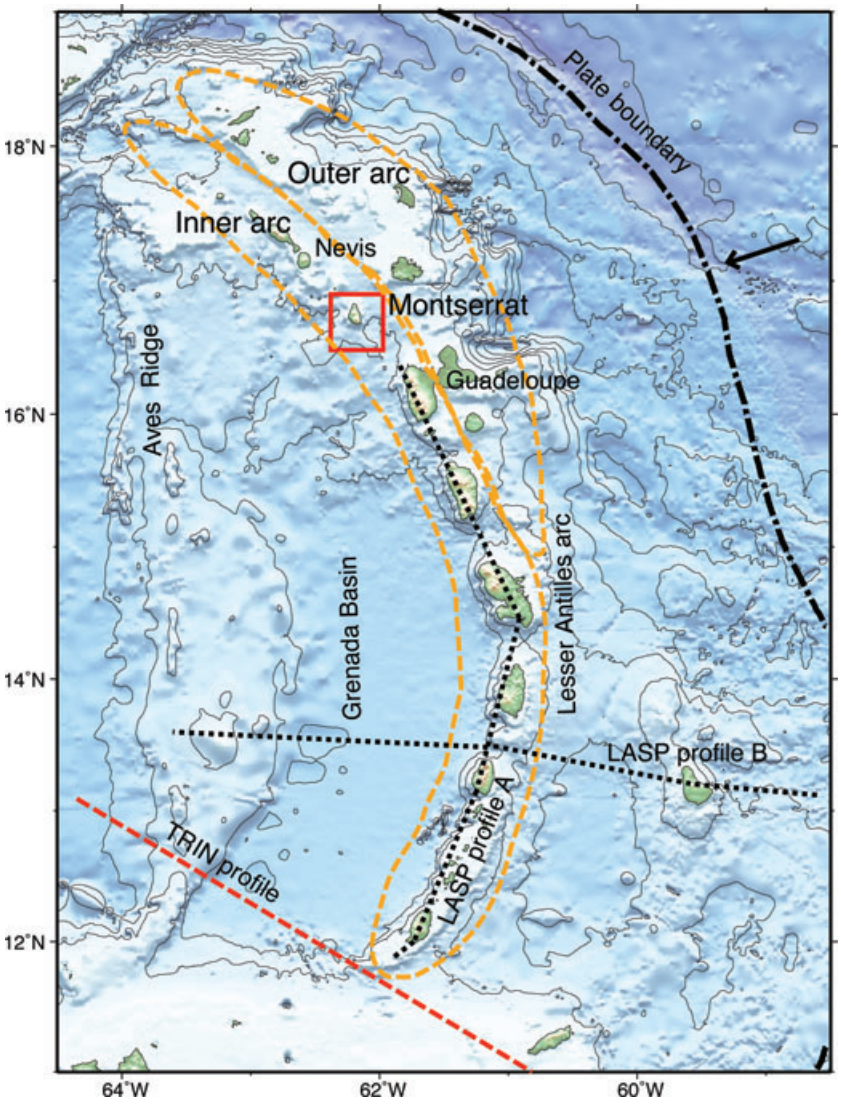

Figure 1. Map of the Lesser Antilles with bathymetry from the GEBCO_08 Grid (http://www.gebco.net) and plate boundaries from the University of Texas PLATES database. The study region is highlighted in red. The red dashed line shows the TRIN profile from the BOLIVAR project (Christeson *et al.* 2008). The black dotted lines show the seismic refraction profiles of the Lesser Antilles Seismic Project (LASP) experiment (Boynton *et al.* 1979). The inner and outer branches of the Lesser Antilles arc are highlighted in orange.

pyroclastic deposits and collapse debris, and is scarred by a sector collapse crater (English Crater) opening to the east, and possibly formed around 4000 yr ago (Roobol & Smith 1998).

1.2 Recent activity

Until 1995, no eruption had been recorded since the first Europeans settled on Montserrat in 1632, but there is evidence that Soufriére Hills was active in the 1500s and the early 1600s, with the formation of Castle Peak dome partially filling English Crater (Young *et al.* 1996). A period of quiescence followed that favoured the colonization of the island, which lasted until the current volcanic episode. The recent eruptive activity was preceded by four precursory periods of increased seismicity, in 1897–1898, 1933–1937, 1966–1967 (Shepherd *et al.* 1971) and 1992–1994 (Aspinall *et al.* 1998). The eruption started in 1995 with a series of phreatic eruptions and has seen three distinct phases, each separated by quiescent periods. The eruptive styles include andesite lava dome growth, vulcanian and subplinian eruptions, pyroclastic flows, sector collapse events, lahars and rockfalls (e.g. Kokelaar 2002). Since the onset of the eruption two thirds of the island have been rendered uninhabitable, including the capital of the island, Plymouth, causing the collapse of the economy and the disruption of most basic services. An exclusion zone has been set up around the island and the south of the island has been evacuated with more than 60 per cent of the population having now left.

1.3 Constraints on the magma system

During the course of the eruption the Soufriére Hills Volcano has been monitored and studied in great detail using geological, geochemical and geophysical methods, and our understanding of its magma system has greatly improved.

The mineral composition of the erupted andesitic magma suggests that the present eruption has been triggered by the injection of hot mafic magma into a cooler silicic magma chamber, causing reheating and remobilization of the crystal-rich resident magma (Devine *et al.* 1998; Murphy *et al.* 1998, 2000; Harford & Sparks 2001). Zellmer *et al.* (2003) and Devine *et al.* (2003) propose that high-Al basaltic magma rises episodically from the deep crust to a shallow magma chamber where it resides and crystallizes to form hydrous andesite melts with high crystal content. The periods of increased seismic activity in 1897, 1933 and 1966 may reflect such magmatic influx without the system as a whole reaching the necessary conditions to trigger an eruption. The precursory seismic activity of 1992 may be related to another such movement of magma from the deeper reservoir into the shallow magma chamber (6–7 km) acting as a trigger for the most recent eruption (Murphy *et al.* 2000). Based on the analysis of Soufriére Hills andesites, Barclay *et al.* (1998) suggest that magma was stored in a water-saturated magma chamber at a minimum depth of 5–6 km prior to eruption. Another lower limit on the depth of the shallow magma chamber beneath Soufriére Hills comes from the distribution of the hypocentres of local earthquakes, with Aspinall *et al.* (1998) concluding that any large magma chamber must be located underneath the main region of seismic activity, at a depth greater than 5 km.

Ground deformation data from the CALIPSO project, including seismometers, dilatometers, tiltmeters and GPS surface measurements, suggest that ground deformation observed during lava-dome collapses can be explained by the pressurization of a magma chamber with 1 km average radius at approximately 6 km depth (Mattioli *et al.* 1998; Voight *et al.* 2006). Elsworth *et al.* (2008) argue that if geodetic and magma flux data are considered together, they are consistent with a coupled system of two magma reservoirs, at 6 and 12 km depth, respectively, connected to the surface and to the deep crust by vertical conduits.

Further constraint on the structure of the island comes from a joint hypocentre/velocity structure inversion performed by Villasenor *et al.* (1996), with data from volcano-tectonic event swarms in 1995 August. Their results showed that the main region of seismic activity underneath Soufriére Hills has a faster *P*-wave velocity than its surroundings.

The large-scale crustal structure of the Lesser Antilles has been investigated with seismic refraction and gravity measurements by Boynton *et al.* (1979) who obtained three 2-D profiles, including one along-strike model of the arc from Guadeloupe southward (Fig. 1). Their model consists of three layers, comprising an 1–5-km-thick upper layer ($V_P = 3.3$ km s^{-1}), a 2–20-km-thick middle layer (average $V_P = 6.2$ km s^{-1}) and a lower crustal layer ($V_P = 6.9$ km s^{-1}) extending down to about 30–35 km depth. The upper layer was interpreted as representing lavas, pyroclastic deposits and sediments, the middle layer as being dominated by plutonic rocks of intermediate composition, and the lower layer as dominantly basic, made up from the igneous crust over which the arc was formed plus gabbros and basic cumulates. The thickness of the crust along the arc was inferred to be 30–35 km, but a recent refraction experiment in the southern Lesser Antilles (Christeson *et al.* 2008) argues that the crustal thickness along the arc is ∼25 km.

2 THE SEISMIC EXPERIMENT

2.1 Setup

The SEA-CALIPSO experiment had the objective of collecting onshore/offshore active-source seismic data to image the upper crust at Montserrat to help constrain the geometry and extent of its magma system. The field programme was conducted in 2007 December and consisted of the installation of a land-sea instrument array and the shooting of 4414 shots from an 8-airgun array over 77 hr. The airgun array had a total volume of 2600 in^3 (42.61 l) and was fired at a constant shot interval of 60 s at a pressure of 2000 p.s.i. (1.382×10^7 Pa). The array was towed at a depth of 10 m and at an average speed of 4.5 knots (2.3 m s^{-1}), giving a mean shot spacing of 139 m. The survey covered an area of 50 × 40 km (Fig. 2).

The instrument array consisted of 28 three-component short-period seismographs (Reftek 130 with 2.0 Hz L22 sensor), 209 one-component geophone seismographs (Reftek 125 with 4.5 Hz L40 sensor), 7 four-channel LC-2000 ocean bottom seismometers (OBSs) and 3 two-channel OBSs. The four-channel OBSs were equipped with a hydrophone and a three-component 4.5 Hz geophone package, and the two-channel OBSs were equipped with a hydrophone and a 2 Hz vertical geophone. Coincident multichannel reflection data were collected during the survey with a 600 m 48-channel streamer.

Reftek 130 sites were chosen to form an evenly spaced regular grid wherever possible, while Reftek 125 (Texan) sites were chosen to be roughly aligned along five across-island transects. Sites were primary chosen to be easily reachable by car, but many instruments had to be deployed on foot or by boat from the sea, especially in the south of the island. Limited access within the exclusion zone resulted in poorer coverage in the south than in the north. The

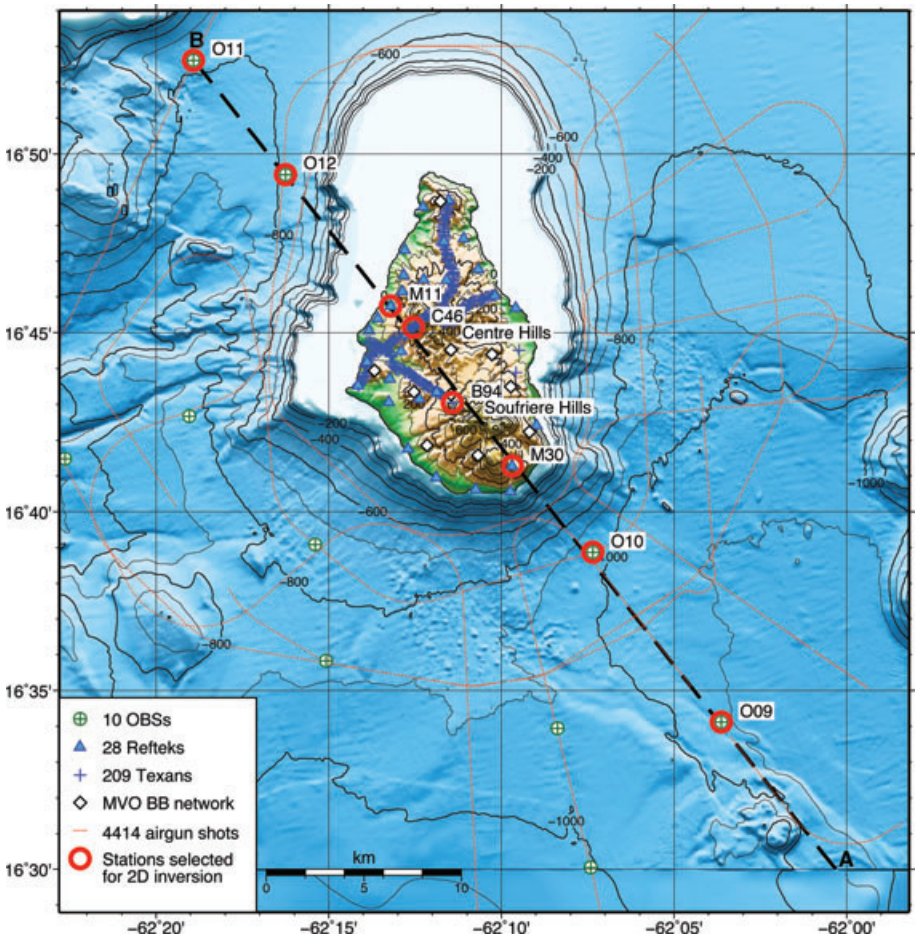

Figure 2. Bathymetric map of Montserrat with SEA-CALIPSO station array and shot positions. The black dashed line marks the position of the 2-D tomographic section presented in this study. The digital elevation model was obtained by merging the GEBCO_08 Grid (http://www.gebco.net) with a detailed elevation model of Montserrat and the surrounding seafloor from Le Friant *et al.* (2004).

permanent Montserrat Volcano Observatory (MVO) seismic network, currently comprising 9 broad-band seismographs and 2 short-period seismographs evenly spaced around Soufriére Hills, also recorded the shots. OBS sites were chosen to avoid potentially hazardous areas, such as submarine canyons, steep slopes, areas covered by recent debris flows, and to be outside the Maritime Exclusion Zone around the south of Montserrat. Sites to the west, on the lee of the island with respect to the predominant trade winds, were preferred to facilitate deployment and recovery of the instruments, which were performed from a 12 m boat, sailing from Basse Terre in Guadeloupe.

2.2 Data

The data quality is generally high, with first arrivals recognizable at up to 50 km offset for the OBSs on both hydrophone and vertical geophone. The horizontal components are also of high quality, suggesting that the instrument-seabed coupling was good. For the land stations data quality depends strongly on the local noise conditions and host materials. Example data sections are shown in Fig. 3.

Land station coordinates have been determined by direct GPS measurement, leading to uncertainties in position of about 5 m. OBS coordinates have been determined by minimizing residuals between observed and calculated first arrivals of seismic waves through the water from GPS located shots near each OBS, leading to OBS position uncertainties of 20–50 m, from shot location uncertainties of up to 20 m.

Identified phases include crustal refracted *P*-wave arrivals and their multiples, refractions turning in the sediments and wide-angle reflections (Fig. 3). In the OBS data (Figs 3a and b) two distinct *P*-wave refractors can be distinguished, with apparent velocities of 2.3 km s^{-1} (layer 1) and 4.0–6.0 km s^{-1} (layer 2), respectively, and giving a first indication of the offshore velocity structure. Phases have been manually picked, from the vertical geophone or hydrophone data, depending on which one presented the best data. Picking uncertainties were estimated visually. For first arrivals at short offset uncertainties are between 20 and 40 ms and at longer offsets between 20 and 100 ms. Reflected phases that are masked by the first arrivals coda have uncertainties of 40 ms. Some gaps are present in the dataset due to short interruptions in shooting caused by sea mammals or other vessels in the vicinity and airgun maintenance.

A subset of the data has been selected for the modelling presented in this paper, consisting of four OBSs and four land stations, approximately aligned on a south-east to northwest line crossing Soufriére Hills and Centre Hills (black dotted line in Fig. 2). Records of the shots on the radial line to the southeast of the island and other isolated shots on the crossings between the selected profile and the shooting track in the northwest have been analysed and traveltimes

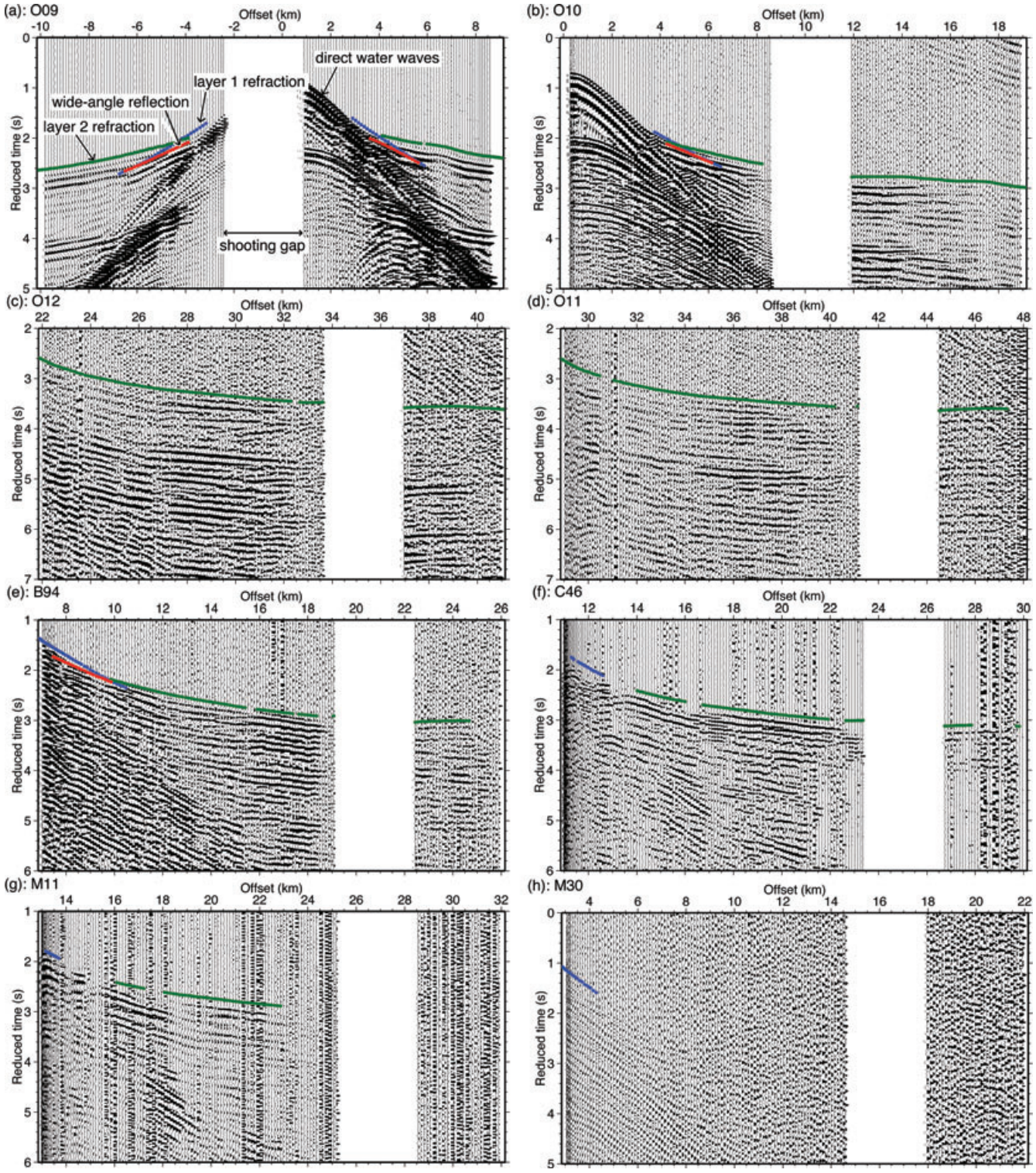

Figure 3. Examples of seismic data plotted as common receiver gathers. Panels correspond to the radial shooting line from point A (right-hand end of the panels) to site O10 (left-hand end) in Fig. 2 recorded on the eight instruments used in the 2-D inversion. (a)–(d) Hydrophone channel recordings of OBS stations O09, O10, O12 and O11. (e)–(f) Vertical geophone recordings of Texan stations B94 and C46. (g)–(h) Vertical component recording of Reftek 130 stations M11 and M30. Synthetic traveltimes calculated through the final velocity model are superimposed on the data (blue: layer 1 refractions; green: layer 2 refractions; red: wide-angle reflections). The white gap present in all panels corresponds to an interruption in shooting due to marine mammals in the vicinity of the guns. A minimum-phase filter with corner frequencies 3-5-20-25 Hz was applied to the data. Amplitudes are normalized with a factor inversely proportional to offset.

have been inverted to obtain a 2-D seismic velocity profile through the island.

A volcanic-arc island is a highly irregular morphological feature, presenting strong heterogeneities with approximately radial symmetry. Although for these reasons a 3-D tomographic experiment is best suited for this kind of study, analysis of a 2-D transect through the centre of the island allows identification and interpretation of many of the key structural features. A 2-D model also allows easier identification of seismic phases after the first arrival and can provide a guide for the inversion of the full 3-D model. The effect of a 2-D approximation is to introduce inconsistencies between different portions of the data where ray paths in the real Earth travelled outside the plane of the 2-D model. To account for these inconsistencies the model has to be smooth. Since in the Earth's crust lateral velocity gradients are normally much smaller than vertical velocity gradients such deviations are usually small.

3 TOMOGRAPHY

3.1 Method

The regularized inversion approach, developed by Hobro *et al.* (2003), has been used. This method allows the data misfit and model roughness to be minimized at the same time to give a minimum-structure model, and it allows the simultaneous inversion of refractions, wide-angle reflections and multichannel seismic data.

The model is defined as a series of layers separated by interfaces. Within each layer the velocity field is continuous and smooth and is defined by interpolating a fine regular grid of velocity parameters with a quadratic B-spline polynomial. In each layer the grid spacing can be independently defined, in this case a 0.5 × 0.5 km grid was adopted. Discontinuities of the velocity field can be introduced as interfaces, represented as smooth and continuous polynomial depth functions.

In our case the starting model consists of a water layer and a crustal layer, with velocity varying only with depth (Fig. 4a). The velocity field was obtained by fitting a series of layers with constant velocity gradient to the data from the four OBSs using a trial-and-error method (Zelt & Smith 1992). The water sound velocity, determined from XBT profiles assuming constant salinity of 35.0 ppt and water density of 1.04 g cm^{-3}, decreases from a value of 1.53 km s^{-1} at the surface to 1.49 km s^{-1} at the sea bottom. Bathymetry and topography along the profile have been extracted with a 200 m interval from the DEM of Le Friant *et al.* (2004).

The inversion process is broken into a series of small linear steps, each composed of a forward modelling and inversion stage. The forward problem is performed following a ray perturbation approach (Virieux & Farra 1991). A fan of rays is first propagated from the receivers to explore the model and estimate shooting angles for each source–receiver pair. Then synthetic traveltimes and Frechét derivatives are calculated using a ray shooting method and traveltime misfits, $\mathbf{r} = \mathbf{t}_{\text{real}} - \mathbf{t}$, are obtained.

The inversion step consists in minimizing the functional Ψ, defined as

$$\Psi(\delta\mathbf{m}) = \delta\mathbf{t}_l^T \mathbf{C}_D^{-1} \delta\mathbf{t}_l + \lambda_m \mathbf{m}^T \mathbf{C}_M^{-1} \mathbf{m}, \quad (1)$$

where $\mathbf{m}$ is the model parameter matrix of the new model, $\delta\mathbf{m}$ is the model perturbation and $\delta\mathbf{t}_l = \mathbf{r} - \mathbf{A}\delta\mathbf{m}$, with $\mathbf{A}$ the Fréchet derivatives matrix. $\mathbf{C}_D$ is the data covariance matrix, describing the uncertainty in traveltime and $\mathbf{C}_M$ is a weighting matrix that measures the model roughness. λ_m is the regularization strength, a parameter that allows the model roughness to be varied during the inversion process. At the beginning λ_m is kept high so that a very smooth model is optimized, then the smoothing is gradually reduced and more detailed structure is allowed to arise until a satisfactory fit to

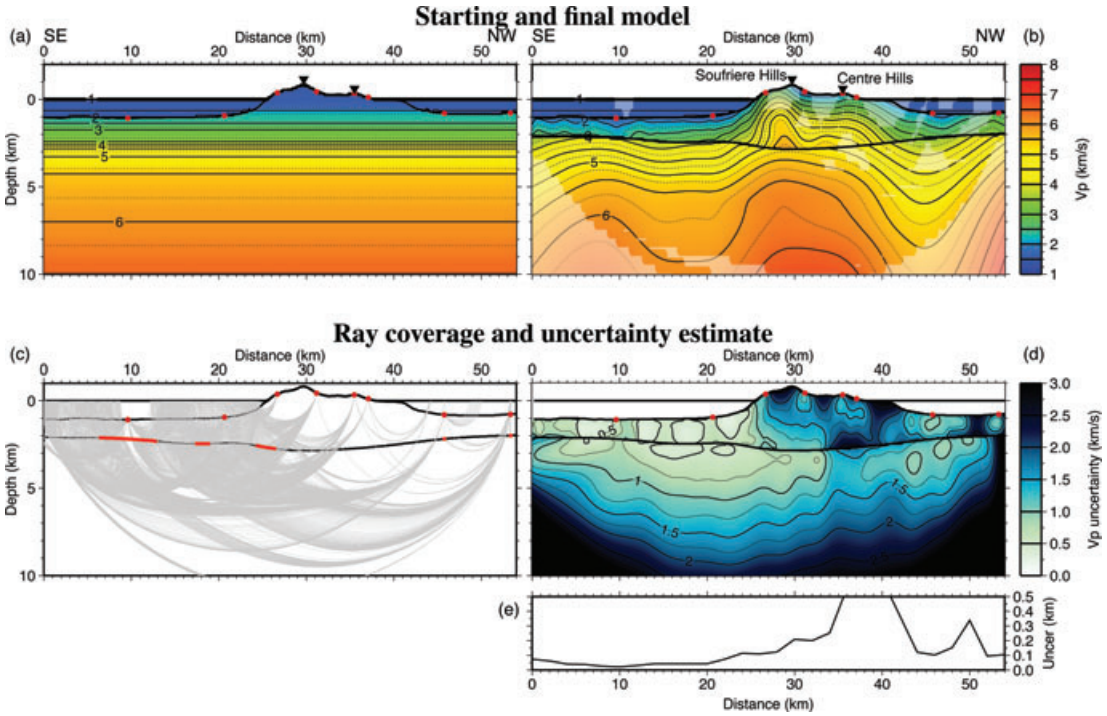

Figure 4. (a) Starting model for inversion process. (b) Final 2-layer model, paler areas are not sampled by rays inverted in the final step. (c) Ray coverage of final model. Segments of the basement interface that are sampled by wide-angle reflections are highlighted in red. (d) Velocity uncertainty estimate. (e) Depth uncertainty estimate for basement interface. Station positions are marked by red dots. Vertical exaggeration is 2:1.

the data is achieved. The functional Ψ is not fully optimized, but at each step it moves towards the minimum while still remaining in the region of linearity. The conjugate gradient method (e.g. Scales & Gersztenkorn 1988) is used to calculate the model update vector.

3.2 Inversion approach

A modified version of the layer stripping approach was adopted, in which layers and interfaces are constrained consecutively in order of increasing depth. The shallowest layer is constrained first by inverting short offset phases. As longer offset phases are introduced, deeper layers are constrained. At each step the current and all previous layers and interfaces are inverted. In the following discussion depth is referenced to mean sea level (MSL) unless otherwise specified.

The simple case of a water layer over a single solid layer was considered first. Only first arrivals were inverted, with no external constraints. The same smoothing levels were assigned to the vertical and horizontal direction. The model roughness was increased until the χ^2 was near the value of 1 for all receivers. Once a satisfactory two-layer model was obtained a flat horizontal interface was introduced to split the solid layer into an upper layer (layer 1), corresponding to oceanic sediments and the volcanic edifice, and a lower layer (layer 2), corresponding to the underlying crust and older sediments. This interpretation is suggested by the identified phases and the values of apparent velocities in the seismic record (Fig. 3). The initial depth of the interface was set at 2.4 km, corresponding to a step in the velocity in the initial model. Refractions turning in layer 1 and wide-angle reflections were used to constrain the upper solid layer and the interface separating it from layer 2. Then refractions turning in layer 2 were introduced, to constrain the lower solid layer. During this step the upper solid layer was also inverted. Since wide-angle reflection picks are sparse, a higher smoothing level was assigned to the basement interface. A lower smoothing level was assigned to the upper solid layer, to account for the expected sharp transition between the oceanic sediments and the volcanic edifice.

4 RESULTS

4.1 Seismic velocity structure

The final velocity model (Fig. 4b) extends 54 km in the horizontal direction and from the top of Soufriére Hills at almost 1000 m elevation to a depth of 10 km below sea level. The ray coverage reaches 10 km depth and is denser on the southeast of the island where shots were fired along a radial line coincident with the segment chosen for the 2-D model (Fig. 4c). Layer 1 comprises a sediment layer and the volcanic edifice, and is characterized by a strong lateral velocity gradient in proximity to the coast. Velocities vary from 1.5 to 3.0 km s^{-1} offshore and from 2.5 to 5.5 km s^{-1} onshore. A high velocity core is imaged under the island, with the two highest velocity regions located under the volcanic edifices of Soufriére Hills and Centre Hills, and also extending into layer 2. Offshore velocities in layer 2 vary from 4.0 km s^{-1} at the top to ∼6.5 km s^{-1} at 10 km depth. Onshore velocities vary from 5.0 to 6.5 km s^{-1}. The interface between layer 1 and 2 is located at a depth of between 2.0 and 2.8 km. This interface is well constrained in the offshore region southeast of the island, where it clearly corresponds to a discontinuity in physical characteristics (velocity contrast up to 1.75 km s^{-1}), but is only loosely constrained beneath the island, where there is no velocity contrast. The thickness of layer 1 ranges from 1 km, far from the island, to a maximum value of 3.6 km under the Soufriére and Centre Hills, both of which have maximum elevations of about 1 km above sea level.

Table 1. RMS residuals in seconds for all phases and stations and total χ^2 for the three inverted phases: L1: layer 1 refraction; L2: layer 2 refraction; WR: wide-angle reflection.

	L1	L2	WR	All
O09	0.014	0.017	0.017	0.016
O10	0.020	0.038	0.013	0.034
O12	0.023	0.031	0.073	0.031
O11		0.022	0.091	0.026
B94	0.029	0.040	0.044	0.039
C46	0.061	0.049		0.051
M11	0.057	0.033		0.040
M30	0.026			0.026
All	0.028	0.032	0.027	**0.033**
χ^2	0.92	0.88	0.49	0.91

4.2 Model evaluation

A quick way to asses the quality of fit of a model to wide-angle seismic data is to calculate the χ^2, defined as the quadratic mean of the ratios between traveltime residuals and their corresponding uncertainties. The initial χ^2 was 308.3. This very high initial value is due to the starting model being fit to OBS data only and the difficulty in fitting both land and OBS data with a laterally homogeneous model. The χ^2 for the final model is 0.91, corresponding to a rms traveltime residual of 0.033 s. The rms residuals for all phases and stations are shown in Table 1.

Uncertainties associated with the velocity values and interface depth were estimated by calculating the *a posteriori* covariance matrix (Hobro *et al.* 2003). Synthetic tests using a smooth model have shown that uncertainties calculated with this method are larger that the difference between the true model and the recovered model by a factor of 2 or more, but they provide a good representation of relative uncertainties (Hobro *et al.* 2003). The calculated uncertainties (Figs 4d and e) are usually under 1.0 km s^{-1} in layer 1, with lower values in the regions of denser ray coverage. In layer 2 uncertainties increase from 0.5 to 1.0 km s^{-1} at 2.0 km depth to over 2.0 km s^{-1} at the bottom of the model. Depth uncertainties for the interface separating layer 1 and 2 are usually under 100 m, but increase under the island where ray coverage is sparser (Fig. 4e) and no wide-angle reflections are observed.

A checkerboard resolution test (Fig. 5) was also performed to estimate the spatial resolution of the final model (e.g. Zelt 1999). A 5 per cent 2-D velocity perturbation, built as the superposition of a sinusoidal function in the *x*- and *z*-direction, was added to the final model. Synthetic traveltimes were calculated for the perturbed model and used as new input data for the inversion process. Two cases were tested: a sinusoidal perturbation with half-wavelength of 6.0 km in the *x*-direction and 2.0 km in the *z*-direction added to layer 1 only (Figs 5a and b) and a 10.0 × 3.0 km perturbation added to layer 1 and layer 2 (Figs 5c and d).

The smaller perturbation is recovered well in the offshore region of layer 1, and less successfully beneath the island. The larger perturbation is resolved well in both layers up to a depth of ∼5 km. As expected resolution is greater to the southeast of the island, where the ray coverage is denser. Perturbation cells are smeared

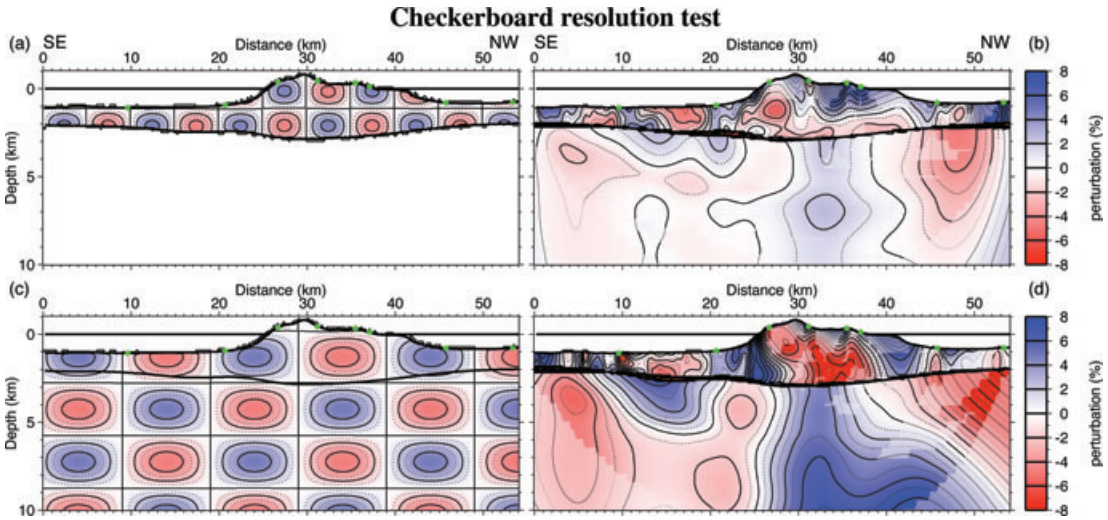

Figure 5. Results from the checkerboard resolution test. Left-hand panels show perturbation added to the final model, right-hand panels show recovered perturbation. (a), (b): 6.0 × 2.0 km anomaly. (c), (d): 10.0 × 3.0 km anomaly. Paler areas are not sampled by rays in the final inversion step. Station positions are marked by green dots. Vertical exaggeration is 2:1.

and sometimes offset along the predominant direction of ray propagation. Resolution beneath ∼5 km depth is poor.

5 DISCUSSION

The velocity model presented in this paper reveals the presence of large lateral velocity variations beneath the volcanic edifice, extending over the entire depth range of the model. Layer 1 is interpreted as a sedimentary layer (V_P = 1.5–3.0 km s^{-1}) plus extrusive and intrusive volcanic material forming the island of Montserrat (V_P = 3.0–5.5 km s^{-1}). Since resolution below 5.0 km is poor, interpretation of the velocity structure in layer 2 has to be cautious. We distinguish two different regions within layer 2. The upper sublayer extends down to 5.0–7.0 km below sea level, with velocities between 3.5 and 6.0 km s^{-1}. It is characterized by strong vertical and lateral velocity gradients and it is interpreted as corresponding to compacted sediments and volcanics. The lower sublayer, with velocities over 6.0 km s^{-1} and a lower velocity gradient, extends to the bottom of the model which is at 10 km depth, and is interpreted to be the top of the crystalline crust, mainly composed of intrusions of intermediate composition. Layer 1 plus the upper sublayer of layer 2 correspond to the upper layer defined by Boynton *et al.* (1979), while the lower sublayer corresponds to the top of the middle layer defined by Boynton *et al.* (1979).

5.1 Volcanic edifice and sediments

In layer 1 the predominant feature of the velocity field is the presence of high *P*-wave velocities beneath the island contrasting with the lower velocity sediments on the flanks and beneath the ocean floor. The velocity contours mirror the topography and suggest that the high velocity region has two cores, below Soufriére Hills and Centre Hills, respectively. The high velocity region is continuous across the interface separating the two layers, but because of the smoothing of the model the two cores cannot be resolved in layer 2, and it is not clear whether they join at depth or remain distinct. The highest lateral velocity gradient is not located under the slope of the submarine shelf but is further inland. The outer portion of the island's edifice, mostly submerged, has a lower velocity than that found under the volcanic centres.

Porosity and pressure play an important role in determining seismic velocities in the sediments and at the top of the crust (e.g. Calvert *et al.* 2008), and a wide range of lithologies can have similar velocities, so velocity variations cannot be related to differences in petrology without the presence of independent constraints. We can distinguish three regions within layer 1: a high-velocity core, an apron, and the sedimentary cover, each characterized by different seismic velocities. Based on the constraints posed by the exposed geology of the Soufriére Hills Volcano, on the identification of numerous noritic xenoliths with hypabyssal textures in the lavas (Kiddle *et al.* 2008), and on geophysical evidence that indicates that the current eruption is fed from a shallow dyke (Mattioli *et al.* 1998; Hautmann *et al.* 2009), this high-velocity core is likely to include a pile of andesitic domes and a system of dykes and sills that represent the feeders for several dome eruptions over the last 170 ka. The exposed geology consists of andesite domes, associated breccias formed by rockfalls and mass wasting, and hydrothermally altered equivalents (e.g. Harford *et al.* 2002). High temperature thermal metamorphism of altered andesite clastic rocks may also play a role in elevating the seismic velocities of the cores.

The seismic velocities observed can be compared to those computed from the effective elastic moduli predicted by the Voigt-Reuss-Hill average (Hill 1952). A representative andesite from Soufriére Hills, composed of 80 per cent phenocrysts and microphenocrysts (52 per cent plagioclase, 19 per cent amphibole, 9 per cent pyroxene and 7 per cent magnetite) and 20 per cent andesite glass (Murphy *et al.* 2000) has a predicted seismic velocity of 6.7 km s^{-1}, when using the values tabulated by Ahrens (1995) for the elastic moduli of the constituent minerals. This value is considerably higher than measured velocities in andesites (e.g. Christensen & Mooney 1995), which have lower values due to finite porosity. Using the Hashin–Shtrikman bounds (Hashin & Shtrikman 1963) it is possible to obtain a rough estimate of the porosity of a rock that is composed by a porous matrix with the same mineral composition as the representative andesite and a water-filled pore space. An andesite with V_p = 5.381 km s^{-1} [the value tabulated by Christensen & Mooney (1995)] is predicted to have a porosity of at least 2.5 per cent and an andesite with *P*-wave velocity of 4.0 km s^{-1} is predicted to have a porosity of at least 8.1 per cent. These values are compatible with porosity measured in samples of recent eruptive products

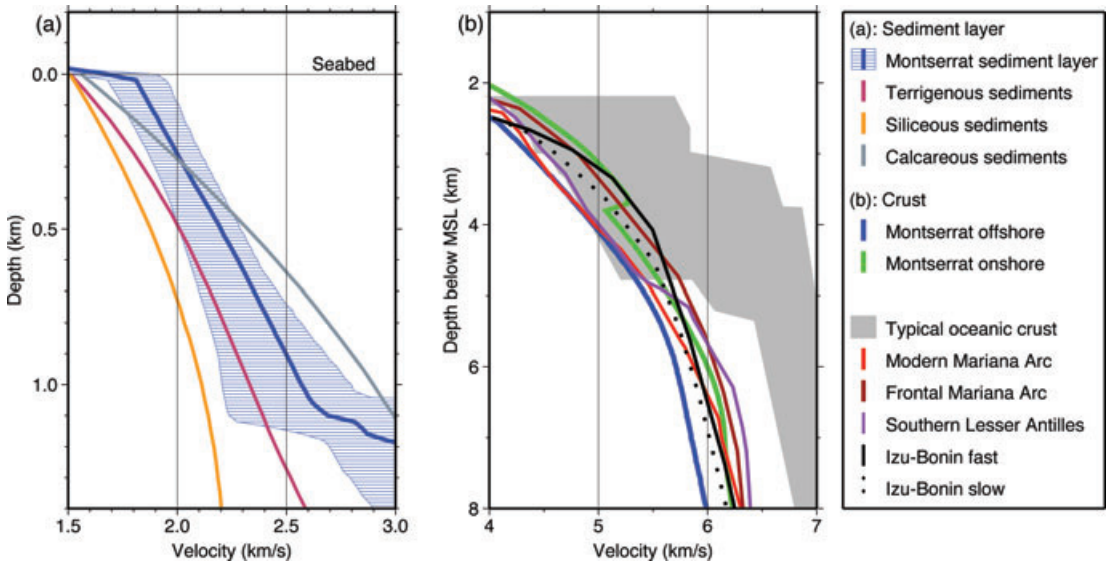

Figure 6. Comparison of vertical velocity profiles from this study and other settings. (a) Velocities in layer 1; profiles are aligned at the seabed. The blue line represents the median model for the offshore region from $x = 2$ to 22 km, the shaded blue area represents the 95 per cent quantile. The brown, orange and grey lines are regression equations fitted to experimental data for terrigenous, siliceous and calcareous sediments, respectively (Hamilton 1980). (b) Velocities in the crust, profiles are aligned at mean sea level. The blue and green lines represent the median models for the offshore region, from $x = 2$ to 26 km, and the onshore region, from $x = 26$ to 37 km, respectively. The onshore velocity profile has been shifted downward by 0.9 km to account for the elevation difference. The shaded grey area is the envelope of typical velocities of mature oceanic crust (59–170 Ma) in the Atlantic Ocean (White *et al.* 1992). The other curves represent average crustal velocity models from different island arcs: the Mariana arc (Calvert *et al.* 2008), the southern Lesser Antilles arc (Christeson *et al.* 2008) and the Izu-Bonin arc (Kodaira *et al.* 2007).

(dome fragments, lavas, bombs, welded breccias and pumice) from Soufriére Hills (Melnik & Sparks 2002).

The lower-velocity apron is made up of material displaced from the top of the volcanoes by eruptions, flank collapses, rockfalls and erosion and deposited on the flanks and on the seabed (Le Friant *et al.* 2004, 2009). This region is characterized by a strong lateral velocity gradient and has velocities that are intermediate between the solid andesite and the submarine sediments ($V_P = 2.5 - 4.0$ km s^{-1}). Different degrees of compaction, grain size, water content and percentage of pelagic sediments could account for the range in seismic velocities observed.

Velocities in the sediment layer in the offshore region are those of normal oceanic sediments ($V_P = 1.5$–3.0 km s^{-1}). These velocities have been compared with those calculated by Hamilton (1980) for terrigenous, silicic and calcareous sediments (Fig. 6a), to constrain the sediment composition. The median model generally falls between velocities typical of terrigenous and calcareous sediments, but exhibits higher velocities in the top 300 m. At very shallow depth velocities are not well constrained because short-offset refractions are obscured by direct water arrivals in the seismic record. In our model the shortest offset refractions turning in the sediments that could be observed bottom out at about 200 m depth. The range of velocities observed is consistent with data from sediment cores collected in the region (Reid *et al.* 1996; Le Friant *et al.* 2008) that suggest that the main sediment components are hemipelagic calcareous and volcaniclastic sediments, interspersed with turbidites. The gradual decrease in velocity with increasing distance from the coast (Fig. 4b) is attributed to a variation in the volcaniclastic content, and to the presence of different volcaniclastic sedimentary facies having different physical characteristics. Coarse grained sediments are expected to be more abundant close to the shelf slope, while fine grained sediments are deposited farther away (e.g. Trofimovs *et al.* 2006).

The interface separating layer 1 and 2 is interpreted as the palaeoseabed at the time when volcanic activity shifted from the outer to the inner Lesser Antilles Arc (∼22 Ma). Far from the island, where layer 1 thickness is about 1200 m, this interpretation gives a mean sedimentation rate of 5.4 cm ka^{-1}. This result is in agreement with sedimentation rate estimates from sediment cores in the Lesser Antilles (Reid *et al.* 1996; Le Friant *et al.* 2008). In the coincident multichannel reflection data, which are not yet fully processed, this interface is rarely associated with a discrete reflector and often obscured by multiples. The interface is depressed under the island, perhaps due to flexure of the underlying lithosphere. Other mechanisms that may be involved are removal of material from layer 2 during volcano growth, compaction of layer 2 material beneath the volcano, tectonic deformation, or a combination of these effects. There is also evidence in the coincident seismic reflection data collected (Kenedi *et al.* 2008) and from the regional-scale bathymetry (Le Friant *et al.* 2004) that a major extensional fault is crossed by our section, corresponding to the rim of the Bouillante–Montserrat graben. This feature may be related to the shallowing of the interface at $x < 10$ km. It is not yet clear whether the wide-angle reflector imaged beneath South Soufriére Hills (at $x = 26$ km in Fig. 4c) corresponds to the same feature as the wide-angle reflector imaged offshore, or whether it is distinct, possibly corresponding to a sill. A single continuous interface was used because the model parametrization adopted requires interfaces to be continuous across the model.

5.2 Layer 2

P-wave velocities at the top of the layer 2 are relatively stable offshore, ranging from under 4.0 to 4.25 km s^{-1}, but increase strongly to over 5.0 km s^{-1} under the volcanic centres. This large variation in

velocity suggests the presence of lateral variations in the chemical composition of the crust. Offshore upper crustal velocities are close to those found in the Modern Mariana arc (Calvert *et al.* 2008) and in the southern Lesser Antilles arc (Christeson *et al.* 2008) and fall at the lower end of the interval of velocities found in typical oceanic crust (Fig. 6b). A similar low-velocity upper crust in the Mariana arc (Takahashi *et al.* 2007) and in the Izu arc (Kodaira *et al.* 2007) has been interpreted as being mainly basaltic in composition, and its low velocity has been attributed to high porosity (Christeson *et al.* 2008). In Montserrat this layer may correspond to volcanic and sedimentary products from the early stages of arc formation on the outer Lesser Antilles arc (Eocene to Miocene) and on the Mesozoic arc, that was the focus of subduction-related volcanic activity before the opening of the Grenada basin and is believed to constitute the substratum over which the Lesser Antilles arc was built (Bouysse *et al.* 1990; Macdonald *et al.* 2000).

In the middle of the section a peak is observed in the isovelocity contours under the island, forming the continuation of the high velocity body constituting the core of the volcanic edifice. Onshore upper crustal velocities are elevated, usually above 5 km s^{-1}. At 5 km depth beneath Soufriére Hills the seismic velocity is ∼6.20 km s^{-1}, compatible with an intermediate, possibly dioritic, composition (Christensen & Mooney 1995). These elevated velocities, may represent an intrusive complex formed over the 300 ka lifetime of the volcano, extending from 2.0 to 6.0 km depth and joining at the top with the volcanic edifice. New intrusions in this complex could be related to the seismic precursors of 1897–1898, 1933–1937, 1966–1967 and 1992–1994 and to the volcano-tectonic seismic activity of the early phase of the current eruption (Aspinall *et al.* 1998), and could represent the source region for andesitic magma in the shallow crust (Harford & Sparks 2001). Elevated velocities are also imaged beneath a small submarine volcano to the southeast of the island (at $x = 5$ km in Fig. 4b) and close to Redonda (at $x = 54$ km), and may also correspond to intrusive complexes. Alternatively, the velocity high at $x = 5$ km may correspond to the rim of the Buillante–Montserrat graben, which is crossed by our section approximately at this point. The extent and nature of these features remain unclear since they are at the edges of the section where the model is not well constrained.

The 6.0 km s^{-1} velocity contour, marking the (arbitrarily defined) upper limit of the lower sublayer, is found at depths of between 4.6 and 10 km, consistent with the value of 6.0–7.0 km found by Christeson *et al.* (2008) in the southern Lesser Antilles. In this depth range velocity uncertainties vary from 1.0 to 2.0 km s^{-1}, leading to uncertainties in the depth of velocity contours of up to 2.5 km, with the assumption that uncertainties are overestimated by a factor of 2. Since high uncertainties characterize this region of the model, only mean characteristics can be inferred. The bulk velocity is significantly lower than that found in mafic oceanic crust at these depths (White *et al.* 1992), suggesting an intermediate or felsic composition. Contemporary models of igneous processes in mature arcs suggest that the silicic magmas (andesites, dacites and rhyolites) are generated predominatly in the lower crust by intrusion and differentiation of basalt with subsidiary partial melting of older crustal rocks (Annen & Sparks 2002; Annen *et al.* 2006). The silicic magmas are then emplaced into the upper crust to form granitoid intrusions, such as tonalite and granodiorites, and shallow magma chambers that supply the arc volcanoes. Such models are supported by geophysical observations (e.g. Harrison & White 2006) and are consistent with our observations.

No evidence of a low velocity zone that may correspond to a large magma body has been found in the upper or middle crust, due perhaps to shallow penetration of rays and poor resolution at depth, but the results of the uncertainty and spatial resolution analysis show that a small (radius <2.0 km) or deep (depth >6.0 km) magma reservoir may have gone undetected in our model. Evidence for the presence of magma bodies under Montserrat may in future emerge from the analysis of wide-angle reflections, from the inversion of *S*-wave arrivals or from waveform amplitude modelling.

Petrological interpretations of seismic velocity models are non-unique and can only provide loose bounds on the chemical composition of the crust (Behn & Kelemen 2003). A realistic lithological interpretation is only possible if other constraints are present. Recent Geological investigations of eruptive products on Montserrat have been focused on the study of the composition of the andesitic magma and the mafic magmatic inclusions (e.g. Zellmer *et al.* 2003). These investigations have provided constraints on the structure and composition of the volcanic edifice and the magma chamber, but little information on the composition of the crust. The study of plutonic nodules found in the erupted andesites (Kiddle *et al.* 2008) may be used to sample the crust under Montserrat and help to constrain the lithological interpretation of our model.

6 CONCLUSIONS

The 2-D inversion of combined refracted and reflected seismic phases from the SEA-CALIPSO experiment provides a valuable constraint on the seismic velocity structure beneath Montserrat and its surroundings. The data set used allows us to image the sedimentary cover and the upper crust up to a depth of 10.0 km, though resolution is poor beneath 5.0 km. The model consists of two solid layers separated by a subhorizontal interface and topped by a water layer. The main features are summarized in the following.

(i) Layer 1 includes the sedimentary cover (V_P = 1.5–3.0 km s^{-1}), of mainly calcareous and volcaniclastic composition, and the island's edifice, divided into a core (V_P = 4.0–5.5 km s^{-1}) and an apron (V_P = 2.5–4.0 km s^{-1}) and has a thickness ranging from 1.0 to 4.0 km. The high velocity region under the island has two distinct velocity highs corresponding to the cores of the volcanic edifices, built of a pile of andesite lava domes and subsequent intrusions.

(ii) The interface separating layer 1 and 2 is located at 2.0 to 2.8 km depth and is interpreted as the palaeoseabed at the onset of volcanic activity on the inner Lesser Antilles arc (∼22 Ma). This interpretation gives a mean sedimentation rate of 5.4 cm ka^{-1}, consistent with published sedimentation rates in the region. Some indication of lithospheric flexure is suggested by the depression of the interface under the volcanic edifice.

(iii) Layer 2 corresponds to the upper 8 km of the crust. The upper sublayer (V_P = 4.0–6.0 km s^{-1}) is interpreted as corresponding to volcanics and sediments from the early stages of arc formation. Under the island the upper crust presents increased velocities that are believed to correspond to an intrusive complex perhaps of intermediate composition. Large uncertainties characterize the lower region of our model. Low bulk velocities are in agreement with petrological models of igneous processes in island arcs that suggest that the upper crust is dominated by granitoid intrusions created by the emplacement of silicic magmas.

ACKNOWLEDGMENTS

We wish to thank the officers, crew and technical staff of the RRS James Cook cruise JC19 for their assistance during the field

work and everybody who contributed to the deployment of the instrument array. The SEA-CALIPSO project was funded by the National Science Foundation (Geophysics, Continental Dynamics, I&F, P&G), the National Environmental Research Council (provision of ship time), the British Geological Survey (BGS), the Incorporated Research Institutions for Seismology (IRIS), Discovery Channel TV and the British Foreign & Commonwealth Office (FCO). We thank two anonymous reviewers for their constructive comments.

REFERENCES

Ahrens, T.J., ed. 1995. *Mineral Physics and Crystallography: A Handbook of Physical Constants,* American Geophysical Union.

Annen, C. & Sparks, R.S.J., 2002. Effects of repetitive emplacement of basaltic intrusions on thermal evolution and melt generation in the deep crust, *Earth. planet. Sci. Lett.,* **203,** 937–955.

Annen, C., Blundy, J.D. & Sparks, R.S.J., 2006. The genesis of intermediate and silicic magmas in deep crustal hot zones, *J. Petrol.,* **47,** 505–539.

Aspinall, W.P., Miller, A.D., Lynch, L.L., Latchman, J.L., Stewart, R.C., White, R.A. & Power, J.A., 1998. Soufriére Hills eruption, Montserrat, 1995-1997: volcanic earthquake locations and fault plane solutions, *Geophys. Res. Lett.,* **25**(18), 3397–3400.

Barclay, J., Rutherford, M.J., Carroll, M.R., Murphy, M.D., Devine, J.D., Gardner, J. & Sparks, R.S.J., 1998. Experimental phase equilibria constraints on pre-eruptive storage conditions of the Soufriére Hills magma, *Geophys. Res. Lett.,* **25**(18), 3437–3440.

Behn, M.D. & Kelemen, P.B., 2003. Relationship between seismic *P*-wave velocity and the composition of anhydrous igneous and meta-igneous rocks, *Geochem. Geophys. Geosyst.,* **4**(5), 1041+—, doi:10.1029/2002GC000393.

Bouysse, P., Westercamp, D. & Andreieff, P., 1990. The Lesser Antilles Island Arc, Tech. Rep. 110, Proc. ODP, *Sci. Results*, College Station, TX.

Boynton, C.H., Westbrook, G.K., Bott, M.H.P. & Long, R.E., 1979. A seismic refraction investigation of crustal structure beneath the Lesser Antilles island arc, *Geophys. J. Int.,* **58**(2), 371–393, doi:10.1111/j.1365-246X.1979.tb01031.x.

Calvert, A.J., Klemperer, S.L., Takahashi, N. & Kerr, B.C., 2008. Three-dimensional crustal structure of the Mariana island arc from seismic tomography, *J. geophys. Res.,* **113,** doi:10.1029/2007JB004939.

Christensen, N.I. & Mooney, W.D., 1995. Seismic velocity structure and composition of the continental crust: a global view, *J. geophys Res.,* **100**(B6), 9761–9788.

Christeson, G.L., Mann, P., Escalona, A. & Aitken, T.J., 2008. Crustal structure of the Caribbean-northeastern South America arc-continent collision zone, *J. geophys. Res.,* **113**(B12), 8104, doi:10.1029/2007JB005373.

Devine, J.D., Murphy, M.D., Rutherford, M.J., Barclay, J., Sparks, R.S.J., Carroll, M.R., Young, S.R. & Gardner, J.E., 1998. Petrologic evidence for pre-eruptive pressure-temperature conditions, and recent reheating, of andesitic magma erupting at the Soufriére Hills Volcano, Montserrat, W.I., *Geophys. Res. Lett.,* **25**(19), 3669–3672.

Devine, J.D., Rutherford, M.J., Norton, G.E. & Young, S.R., 2003. Magma storage region process inferred from geochemistry of Fe-Ti oxides in andesitic magma, Soufriére Hills Volcano, Montserrat, W.I., *J. Petrol.,* **44**(8), 1375–1400.

Elsworth, D., Mattioli, G., Taron, J., Voight, B. & Herd, R., 2008. Implications of Magma transfer between multiple reservoirs on eruption cycling, *Science,* **322,** 246.

Hamilton, E.L., 1980. Geoacoustic modeling of the sea floor, *J. acoust. Soc. Am.,* **68**(5), 1313–1340.

Harford, C.L. & Sparks, R.S.J., 2001. Recent remobilization of shallow-level intrusions on Montserrat revealed by hydrogen isotope composition of amphiboles, *Earth planet. Sci. Lett.,* **185,** 285–297.

Harford, C.L., Pringle, M.S., Sparks, R.S.J. & Young, S.R., 2002. The Volcanic evolution of Montserrat using $^{40}Ar/^{39}Ar$ geochronology, in *The Eruption of Soufriére Hills Volcano, Montserrat, from 1995 to 1999,* Vol. 21, pp. 93–113, eds Druitt, T.H. & Kokeelar, B.P., The Geological Society of London, Memoirs.

Harrison, A.J. & White, R., 2006. Lithospheric structure of an active backarc basin: the Taupo Volcanic Zone, New Zealand, *Geophys. J. Int.,* **167,** 968–990.

Hashin, Z. & Shtrikman, S., 1963. A variational approach to the theory of the elastic behaviour of multiphase materials, *J. Mech. Phys. Solids*, **11**(2), 127–140.

Hautmann, S., Gottsmann, J., Sparks, R.S.J., Costa, A., Melnik, O. & Voight, B., 2009. Modelling ground deformation response to oscillating overpressure in a dyke conduit at Soufriére Hills volcano, Montserrat, *Tectonophysics*, **471,** 87–95.

Hill, R., 1952. The Elastic Behaviour of a Crystalline Aggregate, *Proc. Phys. Soc. Sect. A*, **65**(5), 349–354.

Hobro, J.W.D., Singh, S.C. & Minshull, T.A., 2003. Three-dimensional tomographic inversion of combined reflection and refraction seismic traveltime data, *Geophys. J. Int.,* **152,** 79–93.

Kenedi, C.L. *et al.*, 2008. Volcano-tectonic history of the Island of Montserrat, West Indies, from seismic reflection profiles, Eos Trans. AGU, **89**(53), Fall Meet. Suppl., Abstract V53C-06.

Kiddle, E., Edwards, B., Loughlin, S., Petterson, M. & Sparks, S., 2008. Insights Into the magmatic system and crustal structure at Soufriére Hills Volcano, Montserrat (Lesser Antilles) from plutonic nodules, Eos Trans. AGU, **89**(53), Fall Meet. Suppl., Abstract V51C-06.

Kodaira, S., Sato, T., Takahashi, N., Ito, A., Tamura, Y., Tatsumi, Y. & Kaneda, Y., 2007. Seismological evidence for variable growth of crust along the Izu intraoceanic arc, *J. geophys. Res.,* **112,** doi:10.1029/2006JB004593.

Kokelaar, B.P., 2002. Setting, chronology and consequences of the eruption of Soufriére Hills Volcano, Montserrat (1995-1999), in *The Eruption of the Soufrière Hills Volcano, Montserrat, from 1995 to 1999,*Vol. 21, pp. 1–43, eds Druitt, T. & Kokelaar, B., Geological Society, London, Memoirs.

Le Friant, A., Harford, C., Deplus, C., Boudon, G., Sparks, R.S.J., Herd, R.A. & Komorowski, J.C., 2004. Geomorphological evolution of Montserrat (West Indies): importance of flank collapse and erosional processes, *J. Geol. Soc.,* **161,** 147–160.

Le Friant, A. *et al.*, 2008. Late Pleistocene tephrochronology of marine sediments adjacent to Montserrat, Lesser Antilles volcanic arc, *J. Geol. Soc.,* **165**(1), 279–289.

Le Friant, A., Deplus, C., Boudon, G., Sparks, R.S.J., Trofimovs, J. & Talling, P.J., 2009. Submarine deposition of volcaniclastic material from the 1995-2005 eruptions of Soufriére Hills Volcano, Montserrat, *J. Geol. Soc. Lond.,* **166,** 1–12.

Macdonald, R., Hawkesworth, C.J. & Heath, E., 2000. The Lesser Antilles volcanic chain: a study in arc magmatism, *Earth-Sci. Rev.,* **49,** 1–76(76).

Mattioli, G.S., Dixon, T.H., Farina, F., Howell, E.S., Jansma, P.E. & Smith, A.L., 1998. GPS measurement of surface deformation around Soufriére Hills Volcano, Montserrat from October 1995 to July 1996, *Geophys. Res. Lett.,* **25**(18), 3417–3420.

Melnik, O. & Sparks, R.S.J., 2002. Dynamics of magma ascent and lava extrusion at Soufriere Hills Volcano, Montserrat, *Geol. Soc., Lond., Memoirs*, **21**(1), 153–171.

Murphy, M.D. *et al.*, 1998. The role of magma mixing in triggering the current eruption at the Soufriére Hills volcano, Montserrat, West Indies., *Geophys. Res. Lett.,* **25**(18), 3433–3436.

Murphy, M.D., Sparks, R.S.J., Barclay, J., Carroll, M.R. & Brewer, T.S., 2000. Remobilization of Andesite Magma by Intrusion of Mafic Magma at the Soufriére Hills Volcano, Montserrat, West Indies, *J. Petrol.,* **41**(1), 21–42.

Reid, P.R., Carey, S.N. & Ross, D.R., 1996. Late Quaternary sedimentation in the Lesser Antilles island arc, *Geol. Soc. Am. Bull.,* **108**(1), 78–100.

Roobol, M.J. & Smith, A.L., 1998. Pyroclastic stratigraphy of the Soufriere Hills Volcano, Montserrat—implications for the present eruption, *Geophys. Res. Lett.,* **25**(18), 3393–3396.

Scales, J.A. & Gersztenkorn, A., 1988. Robust methods in inverse theory, *Inverse Problems*, **4,** 1071–1091.

Shepherd, J.B., Tomblin, J.F. & Woo, D.A., 1971. Volcano-seismic crisis in Montserrat, West Indies, 1966-67, *Bull. Volcanol.,* **35,** 143–163.

Shillington, D.J., Van Avendonk, H.J.A., Holbrook, W.S., Kelemen, P.B., &, J., H.M., 2004. Composition and structure of the central Aleutian island arc from arc-parallel wide-angle seismic data, *Geochem. Geophys. Geosyst.,* **5**(Q10006), doi:10.1029/2004GC000715.

Takahashi, N., Kodaira, S., Klemperer, S.L., Tatsumi, Y., Kaneda, Y. & Suyehiro, K., 2007. Crustal structure and evolution of the Mariana intra-oceanic island arc, *Geology*, **35**(3), 203–206.

Trofimovs, J. *et al.*, 2006. Submarine pyroclastic deposits formed at the Soufriere Hills volcano, Montserrat (1995-2003): what happens when pyroclastic flows enter the ocean? *Geology*, **34**(7), 549–552.

Van Avendonk, H.J.A., Shillington, D.J., Holbrook, W.S. & Hornbach, M.J., 2004. Inferring crustal structure in the Aleutian island arc from a sparse wide-angle seismic data set, *Geochem. Geophys. Geosyst.,* **5**(Q08008), doi:10.1029/2003GC000664.

Villasenor, A., Benz, H.M. & Power, J.A., 1996. Three-dimensional P-wave velocity model for Soufriére Hills Volcano, Montserrat, W.I., in *The Soufriére Hills Eruption, Montserrat, Discussion Meeting of the Volcanic Studies Group of the Geological Society,* 27 November 1996, London.

Virieux, J. & Farra, V., 1991. Ray tracing in 3-D complex isotropic media: an analysis of the problem, *Geophysics*, **56,** 2057–2069.

Voight, B. *et al.*, 2006. Unprecedented pressure increase in deep magma reservoir triggered by lava dome collapse, *Geophys. Res. Lett.,* **33,** doi:10.1029/2005GL024870.

White, R.S., McKenzie, D. & O'Nions, R.K., 1992. Oceanic crustal thickness from seismic measurements and rare earth element inversions, *J. geophys Res.,* **19,** 19 683–19 715.

Young, S.R., Hoblitt, R.P., Smith, A.L., Devine, J.D., Wadge, G. & Shepherd, J.B., 1996. Dating of explosive volcanic eruptions associated with dome growth at the Soufrière Hills Volcano, Montserrat, West Indies, in *Second Caribbean Conference on Natural Hazards and Hazard Management,* Kingston, Jamaica.

Zellmer, G.F., Sparks, R.S.J., Hawkesworth, C.J. & Wiedenbrck, M., 2003. Magma emplacement and remobilization timescales beneath Montserrat: insights from Sr and Ba zonation in Plagioclase, *J. Petrol.,* **44**(8), 1413–1431.

Zelt, A.C., 1999. Modelling strategies and model assessment for wide angle seismic traveltime data, *Geophys. J. Int.,* **139,** 183–204.

Zelt, C.A. & Smith, R.B., 1992. Seismic traveltime inversion for 2-D crustal velocity structure, *Geophys. J. Int.,* **108,** 16–34.